Libyan Desert Glass : new field and Fourier Transform InfraRed data

François Fröhlich, Gérard Poupeau, Aïcha Badou, François-Xavier Le Bourdonnec, Yves Saquin, Stéphan Stephan Dubernet, Jacques-Marie Bardintzeff, Monette Veran, David C. Smith, Edmond Diemer

The Meteoritical Society

Meteoritics & Planetary Science 48, Nr 12, 2517–2530 (2013)
doi: 10.1111/maps.12223

Libyan Desert Glass: New field and Fourier transform infrared data

F. FRÖHLICH[1*], G. POUPEAU[1,2], A. BADOU[1], F. X. LE BOURDONNEC[2], Y. SACQUIN[3], S. DUBERNET[2], J. M. BARDINTZEFF[4,5], M. VÉRAN[6], D. C. SMITH[7], and E. DIEMER[†]

[1]Département de Préhistoire, Muséum National d'Histoire Naturelle, UMR CNRS, 7194 CP57 57, rue Cuvier, Paris 75005, France
[2]Université de Bordeaux 3, CRP2A - UMR CNRS IRAMAT 5060, Maison de l'Archéologie, Pessac 33607, France
[3]CEA/Saclay, DSM/Irfu, F-91191 Gif-sur-Yvette Cedex, France
[4]Laboratoire de Pétrographie-Volcanologie/équipe Planétologie, Université Paris-Sud, UMR CNRS IDES 8148, Bât. 504, Orsay Cédex 91405, France
[5]Université de Cergy-Pontoise, IUFM, Cergy-Pontoise 95000, France
[6]Département Histoire de la Terre, Muséum National d'Histoire Naturelle, USM 203, 8 rue Buffon CP 38, Paris 75005, France
[7]Département Histoire de la Terre, Muséum National d'Histoire Naturelle, UMR CNRS 7202, Lab. LMCM, CP 52, 61 rue Buffon, Paris 75005, France
[†]Deceased
[*]Corresponding author. E-mail: frohlich@mnhn.fr

(Received 03 May 2013; revision accepted 30 September 2013)

Abstract–Results are presented of new geological observations and laboratory analyses on Libyan Desert Glass (LDG), a unique kind of impact glass found in Egypt, probably 28.5–29.4 million years in age. A new LDG occurrence has been discovered some 50 km southward of the main LDG occurrences in the Great Sand Sea. From Fourier transform infrared (FTIR) analysis, the molecular structure of LDG is refined and significant differences are shown between LDG specimens and other pure silica glasses (fulgurite, industrial fused quartz, and amorphous biogenic silica) that are related to differences in their structures. The slight variations observed here for the mean Si-O-Si angle between the different glasses are attributed to their thermal histories. With regard to the other glasses analyzed, the LDG infrared spectral parameters point to a higher ratio of discontinuities and defects in the tetrahedral (SiO_4) network. The quantitative mineralogical constitutions of sandstones and quartzites from the LDG geological setting were analyzed by FTIR. Cretaceous sandstones have a specific composition (about 90 wt% quartz, 10% dickite), clearly different from the Paleozoic ones (about 90 wt% quartz, but ≥7% kaolinite). It is shown that the reddish silts bearing the LDG are constituted mainly of microquartz enriched with dickite, whose particle size distribution is characteristic of fluvio-lacustrine deposits, probably Oligocene to Miocene in age. The target rocks, most probably quartz sand, resulted from the weathering (loss of the cementing microquartz) of the Cretaceous sandstones from the Gilf Khebir Plateau with deposition in a high-energy environment.

INTRODUCTION

Since its discovery in the southern Great Sand Sea (southwestern Egypt: Fig. 1; Clayton and Spencer 1934; Spencer 1939), the intriguing blocks of Libyan Desert Glass (LDG) have been the subject of more than 200 papers (e.g., Barnes and Underwood 1976; Storzer and Koeberl 1991; Rocchia et al. 1996; Monod and Diemer 1997; Greshake et al. 2010; Longinelli et al. 2011). Various field investigations have shown that their strewn field covers a circular area of about 21 km diameter (Barakat et al. 1997). Fission-track dating suggests that LDG solidified between 28.5 ± 0.5 and 29.5 ± 0.4 Ma (Gentner et al. 1969; Storzer and Wagner 1977; Storzer and Koeberl 1991; Bigazzi and de Michele 1997; Horn et al. 1997). The structure of this glass (Fröhlich 1989), being that of fused quartz, suggested that LDG resulted from the fast quenching of

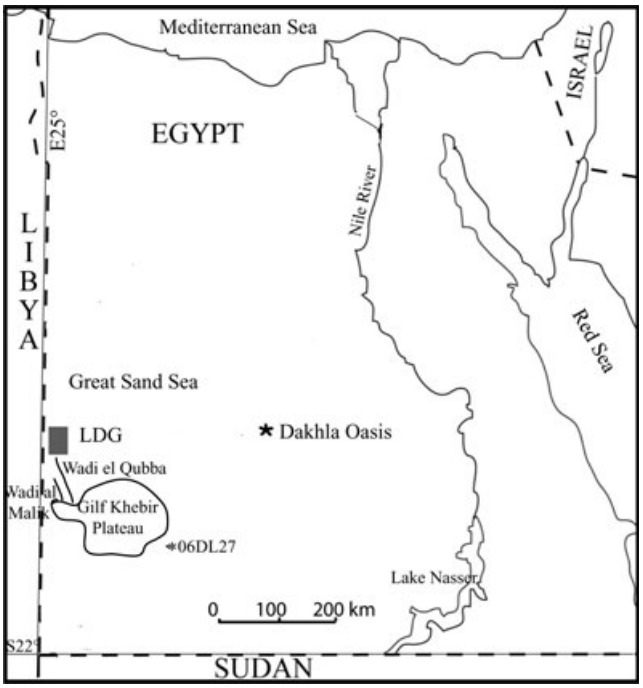

Fig. 1. Location of the LDG strewn field in Egypt.

a silica-rich melt (Rocchia et al. 1996, 1997; Koeberl 1997; Bölitz and Langenhorst 2009; Greshake et al. 2010). The high content of meteoritic components (Rocchia et al. 1996, 1997; Greshake et al. 2010) and the presence of the high-temperature low-pressure silica phase cristobalite in the glass (e.g., Clayton and Spencer 1934; Spencer 1939; Barnes and Underwood 1976) argue strongly in favor of an impact origin. Moreover, the occurrence in LDG of baddeleyite (ZrO_2) (Kleinmann 1969; Storzer and Koeberl 1991), a product of the breakdown of zircon ($ZrSiO_4$) that occurs at a temperature above 1680 °C, clearly demonstrates that very high temperature conditions were attained. Furthermore, Horn et al. (1997) mentioned the occurrence of "skeletal" rutile, which also implied an ultrahigh melting temperature, exceeding 1800 °C. Finally, the mixture of amorphous Al-silicate "spherules" within the silica glass matrix of LDG (Pratesi et al. 2002) suggested temperatures ranging from 1700 to 2100 °C. Thus, five independent mineralogical geothermometers establish the very high temperature nature of the formation of LDG. The total mass of LDG that can be found in this region is estimated between 1.7×10^8 g (Barakat et al. 1997) and 1.4×10^9 g (Weeks et al. 1997). The largest known single specimen, discovered by Théodore Monod and later donated to the French Muséum National d'Histoire Naturelle (MNHN, Paris), weighs 26.5×10^3 g (Diemer 1997).

Kleinmann et al. (2001) recorded shocked quartz near the localities described below. This further consolidates the impact origin of LDG. However, the exceptional richness in SiO_2 (97.5 wt% according to Clayton and Spencer [1934]; between 97.1% and 99.4% according to Barrat et al. [1997]), along with the elemental composition (some Al + alkaline elements) suggested that the impacted rock was a mature quartz-arenite (cf. Fudali 1981). Mesozoic sandstone (formerly called "Nubian" sandstone by Klitzsch 1990) is often cited as a possible terrestrial precursor for LDG (Fudali 1981; Barrat et al. 1997; Rocchia et al. 1997). Svetsov and Watson (2007), Boslough and Crawford (2008), and Longinelli et al. (2011) proposed that LDG did not originate from a meteorite impact, but from a comet airburst. Finally, using various isotopic compositions, Schaaf and Müller-Sohnius (2002) and Longinelli et al. (2011) argued that the target rocks are not Mesozoic sandstones, but sands (Oligocene?) probably originating from the weathering of the Pan-African basement.

However, contemporaneous (Oligocene) astroblemes are absent from the vicinity of the LDG strewn field; furthermore, the specimens do not exhibit typical ejecta morphologies. Thus, despite many studies (e.g., Frischat et al. 2001; Boslough and Crawford 2008; Longinelli et al. 2011), the formation process of LDG remains an open question and calls for continued research. The molecular structure of LDG, as seen with infrared spectroscopy, is typical of a glass (Fröhlich 1989; Rocchia et al. 1996, 1997) with a H_2O content of 0.055–0.166 wt%, whereas it is 0.006–0.060 wt% for other impact glasses, and only 0.002–0.030 wt% for tektites (Beran and Koeberl 1997). One purpose of this paper is to study the variability of the molecular structure of different LDG specimens; another is to study the relevant sediments.

In January 2006, four of the coauthors (E. D., F. F., Y. S., and M. V.) joined a 3-week archaeological expedition into the Egyptian part of the Libyan Desert to survey the geological context of LDG. For this purpose, glass and its surrounding sediments were sampled, along with the acquisition of new observational field data, to acquire new analytical data, mainly using FTIR (Fourier transform infrared spectroscopy), including the powerful quantitative IR analysis of mixtures, and scanning electron microscope (SEM) with energy dispersive spectroscopy (EDS) analyses.

FIELD OBSERVATIONS

LDG is known to occur as centimeter- to decimeter-sized lumps, blocklets, or blocks scattered within an area extending 130 km N–S and 50 km E–W (Spencer 1939; Weeks et al. 1997); here, the term "blocks" is used

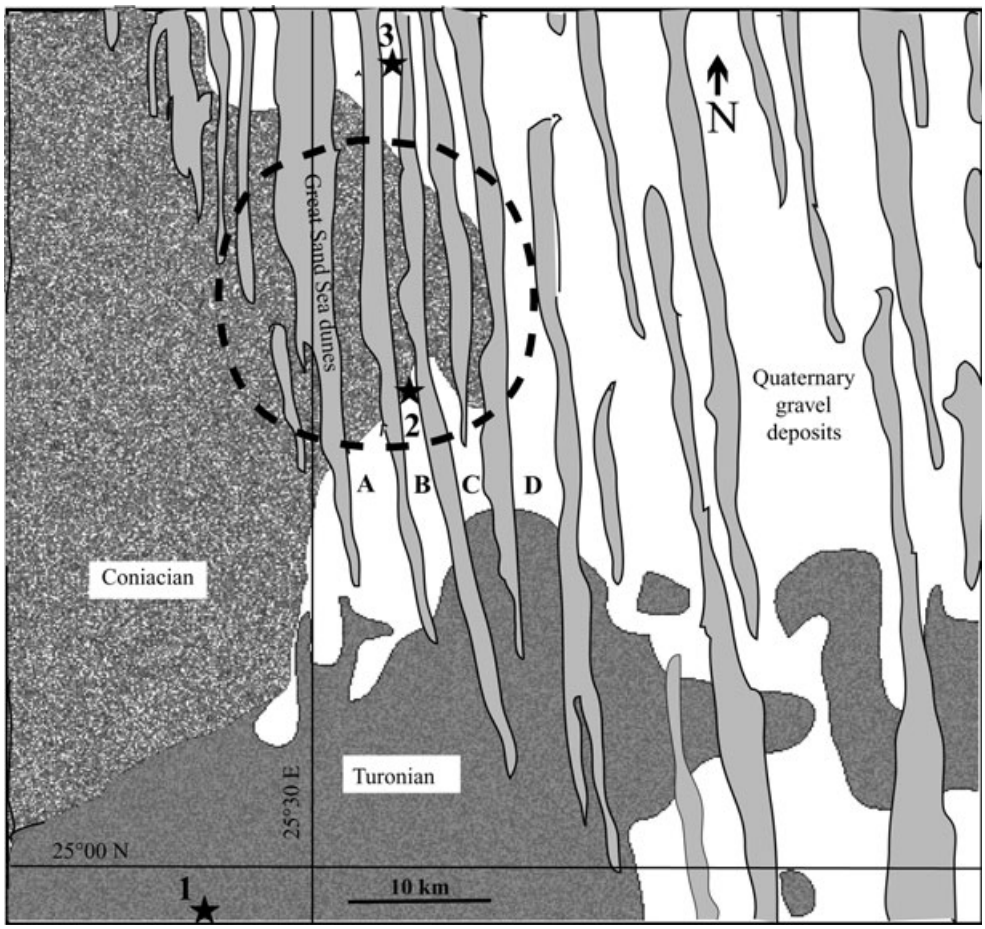

Fig. 2. Schematic geological map of the LDG area in the southern Great Sand Sea (after Klitzsch et al. 1987), with the circular line indicating the strewn field after Barakat et al. (1997). 1) Wadi el Qubba LDG site; 2) corridor B site; 3) northern specimen found during the expedition.

throughout, regardless of the size. According to some other authors, the strewn field is somewhat smaller, e.g., Barakat et al. (1997) considered it to be a roughly circular area of only 20 km in diameter (Fig. 2). This area corresponds to four interdune corridors, called corridors A to D. Each of these corridors is about 5 kilometers wide, has an approximately N-S orientation, and lies at the southern end of the Great Sand Sea (Fig. 2) (Clayton and Spencer 1934; Spencer 1939; Klitzsch et al. 1987; Barakat et al. 1997).

A brief geological survey of the Libyan Desert was made to the west of Dakhla oasis, north of the Sudanese border, and east of the Libyan border (Fig. 1). Mesozoic and Paleozoic sandstones and Quaternary soft deposits were sampled, especially in the Gilf Khebir Plateau and its northwestern valleys (Wadi al Malik and Wadi el Qubba), in the direction of the LDG strewn field. A specific area of 1 km^2 of corridor B (N 25° 17.617′, E 25° 33.414′) was surveyed for 2 days during our expedition (Fig. 2). The terrain (Fig. 3a), gently dipping northward, is a flat surface at an altitude of about 445 m above sea level. The ground surface is covered with rounded very coarse sandstone/quartzite gravels occurring within a layer of coarse sand, which together overlie a fine reddish soft sediment ("silt"; Fig. 3d). The Upper Cretaceous basement (the former called "Nubian" sandstone unit) sporadically outcrops near the dunes. Scattered blocks of wind-worn reddish sandstone/quartzite (ventifacts) occur over the whole surface. The term "reddish" is employed throughout this text, as the colors vary between red, pink, orange, and brown, sometimes lighter, sometimes darker. Some ten centimeter large blocks of massive goethite, including quartzite gravels and sand grains (as seen in thin section), were found in the northern part of this area.

The LDG blocks are partly buried, and, most significantly, only the visible part is wind-worn (Figs. 3b–d). In great contrast, the buried part is coated with silt (Fig. 3c) and is severely pitted (Figs. 3c and 3d) and frequently exhibits tubular cavities, often up to one

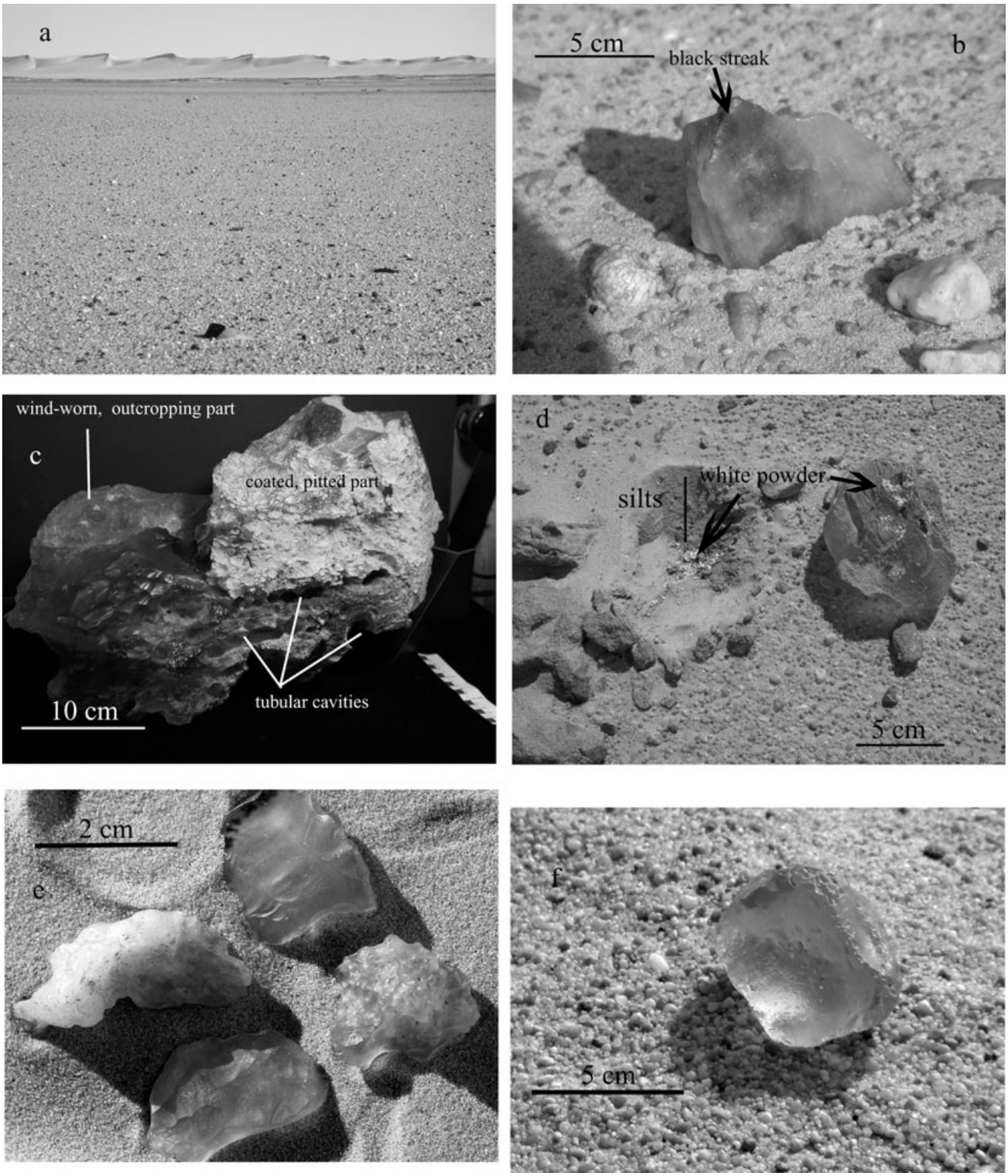

Fig. 3. Field setting and morphology of LDG. a) View of the corridor B with its western barkane dune. b) LDG block with a black streak, cropping out in place. c) The largest LDG specimen known (26.5 kg from the Théodore Monod Collection, MNHN), which exhibits large tubular cavities often filled with red silt. d) Extracted and turned LDG block revealing tubular cavities and a silt coating; red silt appears in place inside the hole in which a white deposit (anhydrite) is seen at the bottom; a coating occurs on the underside of the block. e) Some small LDG specimens from the Wadi el Qubba site. f) The northern specimen, which lies on the ground and is wholly wind-worn.

centimeter in diameter (Fig. 3c); these tubular cavities appear either as entrances to penetrating holes or as transverse sections resembling canals. Some blocks occur entirely exposed, and then their whole surface is wind-worn (Fig. 3f); thus, on exposed faces, the tubular cavities have been mostly eroded away by wind and only traces remain as grooves that are effectively indistinguishable from usual conchoidal wind-weathering features. In some places, a white powder occurs below the LDG blocks (Fig. 3d).

Some of the LDG blocks display brown to black parallel zones or streaks (Fig. 3b). Most of these observations correspond with the first descriptions by Clayton and Spencer (1934), Spencer (1939), and Greshake et al. (2010); the last paper identified some trace elements in the colored zones ("schlieren") deduced to be of terrestrial origin. According to Rocchia et al. (1997), these dark streaks exhibit a significant content of extraterrestrial constituents.

More LDG blocks were not found in corridor B north of the surveyed area, apart from a single small (50 mm; Fig. 3f) wind-worn block that was found lying on the ground surface at an elevation of 382 m at locality N25° 37.287′, E25° 31.971′ (Fig. 1). It is possible that this block might have been transported there, perhaps by Prehistoric people. LDG is known to have been used for lithic industries from Paleolithic time (Clayton and Spencer 1934; Fröhlich et al. 2009).

However, during a stop at a Neolithic occupation site, indicated by many sandstone artifacts lying on the bank of a former Holocene river, our expedition discovered some small centimeter-sized LDG blocks (Fig. 3e), with only one artifact (a broken blade) made from LDG (Fröhlich et al. 2009). This new occurrence (N24° 52.189′, E25° 27.044′, 538 m in elevation) is located about 50 km south of the main LDG occurrences of the Great Sand Sea corridors in Wadi el Qubba (Figs. 1 and 2), the large valley originating from the Gilf Khebir Plateau. This is the southernmost LDG occurrence ever found. These small LDG blocks were also found to be partly or completely buried inside a reddish silt horizon. They exhibit the same types of structures as those in the corridor B prospected area described above.

MATERIALS AND METHODS

Materials Analyzed

The analyzed LDG blocks were all collected during our expedition. The samples collected in corridor B weighed between 60 g and 715 g; the Wadi el Qubba specimens weighed 3 g each. The following samples were analyzed for comparison: a specimen of fulgurite (quartz sand fused by the effect of lightning) collected in the Great Sand Sea (N26° 42.50′, E26° 28.08′), a pure silica glass (pure fused quartz) used in the microelectronics industry (Quartz & Silice, St. Gobain Co.), and amorphous biogenic silica (a sponge spicule dredged in the southern Indian ocean: Fröhlich 1989).

Soft sediments, sandstones, and quartzites related to LDG were also collected and analyzed:

1. Two quartzites and one sandstone from corridor B; two sandstones from Wadi el Qubba; two sandstones from Wadi al Malik; and one sandstone from the east of the Gilf Khebir Plateau (Fujini cave).
2. Silts bearing LDG from corridor B (five samples) and Wadi el Qubba (one sample); seven silts coating LDG lumps; a third locality of soft sediments was sampled from an ancient lake (with a Neolithic occupation) represented by Holocene lacustrine deposits in the central Libyan Desert (N23° 48.31′ E27° 17.13′, about 200 km S.E. of Wadi el Qubba; Fig. 1).
3. Seven samples of reddish silt coating LDG blocks from corridor B; one sample of silts coating the MNHN Théodore Monod 2650 g LDG block (Fig. 3c); and one sample of silts infilling its tubular cavities (Fig. 4c).
4. Two samples of sands, from the Great Sand Sea (80 km northward of the corridor B site) and from a dune barcane between corridors B and C.

Analytical Procedures

The mineralogy of the LDG samples was determined by Fourier transform infrared spectroscopy (FTIR), petrographical microscope examination, and scanning electron microscope-energy dispersion spectrometry (SEM-EDS). FTIR was used in transmission mode using the KBr pellet method adapted to quantitative analyses according to the Beer–Lambert Law (Fröhlich and Leclaire 1981; Pichard and Fröhlich 1986; Fröhlich 1989). The analyses were performed on splinters obtained by breaking the specimens under their surface, to prevent contamination with silts or sands. The samples were mechanically ground using acetone in an agate mortar with three small agate balls. To prevent structural changes due to heating, grinding was performed in a refrigerated area. A particle size less than the shorter wavelength (2.5 μm) is required to avoid scattering IR radiation and to apply the Beer–Lambert law (Duyckaerts 1959). The grain size was verified on smear slides and under a petrographical microscope. The powdered samples were mixed with KBr in the proportion 400:1 by weight to yield a standard dilution of 0.25%. A 300 mg pellet (thus containing 0.75 mg of sample) was made by pressing the mixture in a vacuum die with up to 10^4 kg cm^{-2} of compression. Weighing was performed with an accuracy of 10^{-5} g.

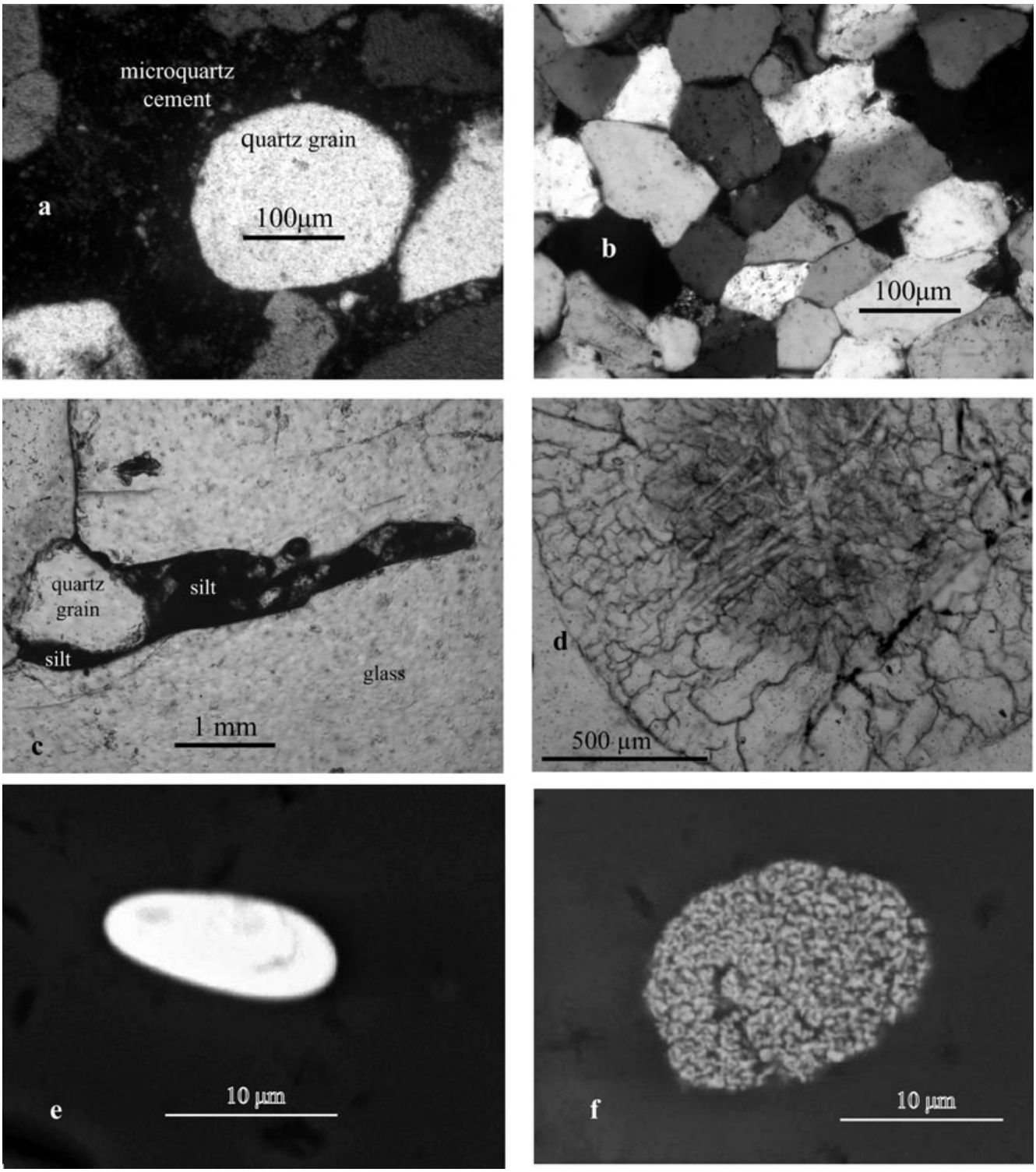

Fig. 4. Thin sections. a) Wadi al Malik sandstone: sand quartz grains cemented with microquartz (polished thin section observed under crossed polarized transmitted light [XPL]). b) Corridor B Turonian quartzite (polished thin section observed under XPL). c–f) Polished thin section of a LDG specimen (06DL66c) from corridor B. c) Tubular cavities filled with silt (black), the opening being blocked by a larger quartz grain (observed under plane polarized transmitted light [PPL]). d) A close-up view of the texture of an inclusion of a cristobalite sphere (observed under PPL). e) A quenched ovoid melt of a previous crystal of monazite (SEM backscattered electron image); present structure unknown. f) A previous zircon crystal transformed into a mixture of baddeleyite (white) and silica glass (dark) (SEM backscattered electron image).

The pellets were analyzed with a Bruker VECTOR 22 FTIR spectrophotometer at a 2 cm^{-1} resolution and an accumulation of 32 scans of 2 s each. The weight% of each component was computed from the absorbance of its specific absorption bands, with reference to the MNHN mineral IR data bank (IR spectra of a 0.75 mg standard mass of pure minerals), according to the Beer–Lambert law:

$$c_x = A_x/\alpha l$$

where A_x is the absorbance (intensity) of a specific band, measured on the spectrum, α = molar extinction coefficient (a constant), l = optical path length (here, the pellet thickness, a constant: 0.83 mm), c_x = the concentration of the constituent in a mixture. Weight% values of a component were computed with reference to the absorbance A of 0.75 mg mass of pure mineral:

$$W\%_x = (A_x/A) \times 100$$

It was experimentally shown from calibration curves that the accuracy of c_x depends on the baseline position (Pichard and Fröhlich 1986). Thus, the overall uncertainty is obtained by computing the absorbances from the two extreme positions of the baseline.

For silica phases, four spectral parameters of the absorption bands that give good indications of the three-dimensional geometry of the (SiO_4) tetrahedra are taken into account here:

1. The wave number v (stretching vibration modes) or δ (bending vibration modes);
2. The absorbance A, according to the Beer–Lambert Law (in arbitrary units), related to the quantity of elemental vibrators;
3. The half-width Δv (= width in cm^{-1} of the absorption band at half absorbance), related to the dispersion of the values of the frequency of a vibration mode;
4. The integrated intensity I (surface of the band, in arbitrary units), which corresponds to the sum of the total energy involved in this vibration mode. The I values were not obtained here with the OPUS Brucker software, but by computing $A \cdot \Delta v$, a good approximation for quite pure Lorentzian/Gaussian bands, and to avoid the deformations of a band, due to weak overlapping bands (e.g., here, water absorptions by KBr).

Concerning the rocks related to LDG, wt% values were obtained from the following absorption bands: 798 cm^{-1} (quartz), 3695 cm^{-1} (kaolinite), 3700 cm^{-1}/ 3654 cm^{-1} (dickite), 878 cm^{-1} (calcite), 595 cm^{-1} (anhydrite), 3553 cm^{-1} (gypsum).

Sandstones were also analyzed on thin polished sections under a Bruker Hyperion 2000 FTIR microscope, and mineral spatial distributions were mapped (in specular reflexion mode) under OPUS 6.5. The kaolinite minerals were mapped with their specific OH stretching absorption band near 3695 cm-1 (2.7 μm in wavelength), and with a lateral resolution of 30 μm. Scanning electron microscope (SEM) observations and complementary analyses were performed at the Centre de Recherche en Physique Appliquée à l'Archéologie (CRP2A, Bordeaux) with a scanning electron microscope JEOL JMS 6460 LV operating at 20 kV equipped with an Oxford Industries INCAx-sight energy dispersive spectrometer (resolution: 128 eV at 5.9 keV).

Grain size analyses were performed with a laser granulometer Malvern Instruments Mastersizer 2000 with a Hydro 2000MU device.

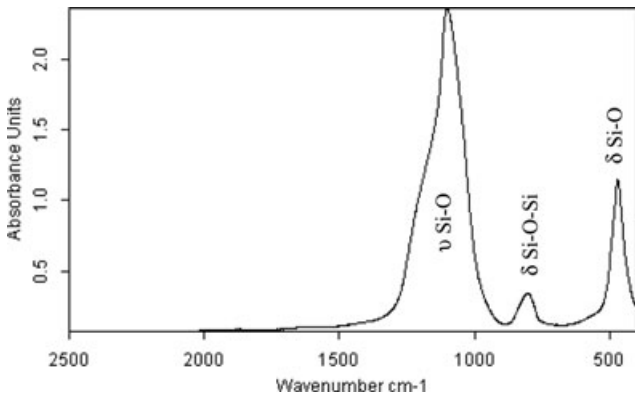

Fig. 5. A representative infrared spectrum of an LDG block (specimen 08600, from corridor B; T1Table) showing no bands other than the expected three key bands of pure SiO_2 glass centered at 1100 cm^{-1} (Si-O stretching mode), 800 cm^{-1} (Si-O-Si bending mode), and 471 cm^{-1} (Si-O bending mode). 0.75 mg analyzed in a 300 mg KBr pellet.

RESULTS

LDG

All LDG IR spectra (Fig. 5) exhibit the three IR-active absorption bands typical for condensed (SiO_4) tetrahedra that are predicted by theoretical considerations. The bands near 1100 and 471 cm^{-1} are assigned to degenerated vibration modes of the (SiO_4) tetrahedral unit, respectively, stretching (ν Si-O) and bending (δ Si-O) (Lecomte 1949). The δ Si-O band is quite stable at 471–472 cm^{-1} for amorphous phases. The wave number of the ν Si-O band is affected by the surroundings of the unit tetrahedron (Lecomte 1949); for crystalline silica phases (e.g., quartz, cristobalite, opal-CT), it is regarded as the envelope of several, poorly resolved bands; then Δv and I are less significant than for amorphous phases. For LDG samples and fulgurite, the

Table 1. Infrared parameters for different amorphous silica phases and LDG blocks from corridor B and Wadi el Qubba.

	Si-O					Si-O-Si				
LDG	δ	υ	*A*	Δυ	*I*	δ	*A*	Δυ	*I*	Ω
Green, translucent 08606[a]	471	1103	2.225 ± 0.005	153.0	341.0 ± 1.0	805	0.232 ± 0.002	64.5	15.0 ± 0.2	4.38 ± 0.02
Green, translucent 09893[a]	471	1103	2.115 ± 0.010	163.0	344.5 ± 1.5	804	0.232 ± 0.002	63.5	14.7 ± 0.1	4.27 ± 0.02
Green, translucent 09892[a]	471	1103	2.351 ± 0.013	151.5	356.0 ± 2.0	805	0.232 ± 0.008	64.5	15.0 ± 0.5	4.20 ± 0.13
Clear, translucent 08600[a]	472	1106	2.670 ± 0.010	145.5	388.5 ± 0.7	805	0.257 ± 0.002	62.0	15.9 ± 0.2	4.09 ± 0.02
White, opaque 08603[a]	472	1104	2.580 ± 0.020	143.0	369.0 ± 3.0	803	0.251 ± 0.006	62.0	15.4 ± 0.4	4.20 ± 0.12
Black vein in a green lump 08601[a]	472	1103	2.262 ± 0.012	152.5	346.0 ± 1.0	802	0.226 ± 0.002	65.0	14.7 ± 0.2	4.25 ± 0.05
Pink, translucent 08602[b]	472	1102	2.435 ± 0.005	151.0	368.1 ± 0.5	806	0.233 ± 0.003	65.0	15.2 ± 0.2	4.13 ± 0.05
Pink, translucent 09891[b]	472	1104	2.324 ± 0.012	155.0	360.0 ± 2.0	805	0.226 ± 0.006	66.5	15.0 ± 0.4	4.15 ± 0.15
Fulgurite (lechatelierite) 09887	471	1103	2.523 ± 0.004	151.0	381.7 ± 0.7	804	0.256 ± 0.006	65.5	16.8 ± 0.4	4.40 ± 0.10
Microelectronic fused quartz 08604	471	1101	2.655 ± 0.007	146.0	387.6 ± 1.0	806	0.265 ± 0.008	67.0	17.8 ± 0.5	4.60 ± 0.10
Amorphous, biogenic silica	470	1100	2.080 ± 0.010	125.0	259.0 ± 1.0	800	0.190 ± 0.010	52.0	10.0 ± 0.5	3.84 ± 0.20

υ = stretching vibration mode (cm^{-1}); δ = bending vibration mode (cm^{-1}); A = absorbance (arbitrary units); Δυ = half-width (cm^{-1}); *I* = integrated intensity (cm^2 mol s^{-1}); Ω = I (Si-O-Si at 800 cm^{-1})/I(Si-O at 1100 cm^{-1}); 0.75 mg analyzed in a 300 mg KBr pellet.
[a]Great Sand Sea, corridor B.
[b]Wadi el Qubba.

wave number of this band is not very variable around 1103 cm^{-1}, whereas the wave number values for fused quartz and amorphous biogenic silica are lower, respectively, 1101 and 1100 cm^{-1}. The absorbance, the half-width, and the integrated intensity vary rather widely, whereas they are stable for crystalline phases.

The third, weaker band, near 800 cm^{-1}, is assigned to a vibration of the bridging oxygen atom in the plane of the Si-O-Si bonds, between the adjacent tetrahedra (Lecomte 1949). The relative motion results in a deformation of the Si-O-Si angle in the direction of its bissectrix (Parke 1974). The different LDG specimens analyzed exhibit wave number values noticeably higher and variable around 804 cm^{-1} ± 2 cm^{-1}, the higher values being observed for fused quartz and the Wadi el Qubba LDG specimen, the lower for amorphous biogenic silica. Taking into account the LDG SiO_2 content variability that affects the absorbance and the integrated intensity of each absorption band, the index Ω ($I_{\text{(Si-O-Si at 800 cm-1)}}/I_{\text{(Si-O at 1100 cm-1)}}$) was computed by Gendron-Badou et al. (2003) as this provides a good indication of the structural continuity regardless of the SiO_2 content. As seen in Table 1, the IR parameters of the seven LDG samples from the Great Sand Sea are remarkably consistent with $\Omega = 4.23 \pm 0.15$, whatever their color and general appearance, The IR parameters of the two Wadi el Qubba samples are also consistent with each other, but differ slightly from those of the Great Sand Sea, essentially by a lower Ω value (4.14 ± 1.00). On the contrary, fulgurite and pure fused silica exhibit the highest Ω index (that reaches 4.60), *A*, Δ*v*, and *I* values for the Si-O-Si band being larger than for most of the other samples. The lowest values for all spectral parameters ($\Omega = 3.84$) are observed for amorphous biogenic silica, due to an additional band at 950 cm^{-1} (Si-OH bonds) which accounts for one in four OH for O substitutions at the apex of (SiO_4) tetrahedra (Fröhlich 1989; Gendron-Badou et al. 2003).

In polished thin sections, LDG appears as a homogeneous glass with spherical bubbles and mainly tubular cavities (Fig. 3c). Sometimes they are at least partly filled with sand grains and/or hardened silt (Fig. 4c). The millimeter-sized (and smaller) whitish polycrystalline spherical inclusions visible inside the LDG volume were identified by FTIR (and also by Raman spectroscopy) as cristobalite concentrations (Fig. 4d). Other mineral inclusions were detected by SEM in BSE mode (backscattered electrons) and determined by EDS. These included melted crystals (deduced on the basis of their elliptical form) of monazite, a rare earth element (REE) phosphate (Fig. 4e) depleted or totally lacking in phosphorus as

Table 2. Weight percent abundances of minerals in sediments associated with LDG, as determined quantitatively by FTIR.

Rock type	Sample	Quartz	Kaolinite	Dickite	Calcite	Anhydrite	Gypsum	Total
Reddish silts bearing LDG								
[a]	06DL65	86.5 ± 1.0	–	4.5 ± 0.1	2.4 ± 0.4	–	–	93.4
[a]	06DL71	85.2 ± 0.6	–	9.5 ± 1.0	2.0 ± 0.2	–	–	96.7
[a]	06DL76a	91.0 ± 0.5	–	4.7 ± 0.7	traces	–	–	95.7
[a]	06DL89b	100.0 ± 0.5	–	traces	–	–	–	100.0
[a]	06DL73	84.5 ± 0.5	–	14.5 ± 1.0	–	–	–	99.0
[b]	06DL60	80.0 ± 0.5	–	18.5 ± 1.0	traces	–	–	98.5
Théodore Monod block								
Silts filling tubular cavities	9796	67.8 ± 0.3	–	25.0 ± 1.0	–	–	3.5 ± 0.7	96.3
Coating silt	9797	76.0 ± 0.5	–	18.0 ± 0.5	4.6 ± 0.1	–	–	98.6
Silts coating LDG lumps								
[a]	06DL63	79.3 ± 03	–	12.5 ± 1.0	1.3 ± 0.1	–	–	93.1
[a]	06DL64	78.0 ± 0.5	traces	15.0 ± 1.0	1.8 ± 0.2	–	–	94.8
[a]	06DL72a	78.5 ± 0.5	traces	13.5 ± 1.5	traces	5.0 ± 0.5	traces	97.0
[a]	06DL74	96.0 ± 0.5	traces	5.0 ± 1.0	traces	–	–	101.0
[a]	06DL75	87.0 ± 0.5	1.0 ± 0.5	5.0 ± 0.5	1.5 ± 0.5	–	–	94.5
[a]	06DL89	98.0 ± 1.0	–	1.5 ± 0.5	traces	–	–	99.5
White fines below LDG lump[a]	06DL72b	traces	traces	10.0 ± 1.0	traces	73.0 ± 1.0	7.0 ± 0.5	90.0
Holocene lacustrine deposits	06DL27	19.5 ± 0.5	75.0 ± 1.0	–	–	–	–	94.5
Mesozoïc sandstones								
Turonian quartzite[a]	06DL68a	94 ± 0.6	–	–	–	–	–	94.0
Turonian/Coniacian quartzite[a]	06DL68b	98.0 ± 1.0	–	2.0 ± 0.5	–	–	–	100.0
Turonian/Coniacian sandstone[a]	06DL68c	88.0 ± 1.0	–	10.5 ± 0.5	–	–	–	98.5
Turonian/Coniacian quartzite[a]	06DL68e	100.0 ± 1.0	–	–	–	–	–	100.0
Turonian reddish sandstone[b]	06DL62	92 ± 0.5	traces	8.0 ± 1.5	traces	–	–	100.0
Upper Cretaceous sandstone[c]	06DL52	85.5 ± 0.5	–	14.5 ± 0.5	–	–	–	100.0
Paleozoïc sandstones								
Devonian white sandstone[c]	06DL57	89.7 ± 0.7	7.4 ± 0.4	–	–	–	–	97.1
Devonian white sandstone[d]	06DL48	87.5 ± 0.7	4.0 ± 0.1	–	–	–	–	91.5

[a]Corridor B.
[b]Wadi el Qubba.
[c]Wadi al Malik.
[d]East of Gilf Khebir. 0.75 mg analyzed in a 300 mg KBr pellet.

seen on their EDS spectra, according to the three domains analyzed (in wt%: Al = 0.2–0.8%, Si = 15.0–26.0%, O = 36.2–37.0%, P = <0.1–9.0%, Ca = <0.1–0.4%, La = 8.4–9.9%, Ce = 14.0–16.9%, Pr = <0.1–1.6%, Nd = 5.9–6.5%, Sm = <0.1–1.0%, Gd = <0.1–0.8%, Th = 3.8–5.8%), and zircon ($ZrSiO_4$) transformed into a mixture of baddeleyite (ZrO_2) and lechatelierite (Fig. 4f); both of these mineralogical processes require great heating.

Surrounding Sediments

Sandstones and Quartzites

As seen in thin sections, Mesozoic sandstones (the former "Nubian" sandstones; Klitzsch 1990) are made up of coarse rounded quartz grains cemented with a high proportion of microquartz (Fig. 4a). Quantitative FTIR analysis of our samples (Table 2) shows a high quartz content (81–100 wt%) for both Mesozoic and Paleozoic sandstones, with a significant content of clay minerals (3.5–10 wt%) of the kaolinite group (that includes dickite and halloysite). However, there is a significant difference, with the clay mineral species being kaolinite *s.s.* for Paleozoic sandstones, and dickite for Mesozoic sandstones. Dickite often grows from kaolinite by thermal or weathering evolution (Ruiz Cruz 1998; Ip et al. 2008) and is characterized by large, well-crystallized crystals. Sandstones mapped under a FTIR microscope show that clay minerals are uniformly dispersed within the microquartz matrix. The Turonian quartzites from the corridor B are quite different and, in thin section, they exhibit no microquartz cement, but just a mosaic of contiguous isometric angular quartz grains (Fig. 4b).

Soft Sediments

The coarse sands overlying the reddish silts consist of rounded quartz and quartzite grains of millimeter to

Table 3. Grain size distribution of silts and sands, expressed in % volume of total specimen.

	Clay fraction (0.1–2 μm)	Silts (2–40 μm)	Fine sand (40–200 μm)	Coarse sand (200–2000 μm)	Finest size (μm)	Coarsest size (μm)
06DL27[a]	57.0	39.5	3.5	n.d.	0.04	140
06DL60[b]	25.0	55.0	17.5	2.5	0.06	400
06DL65[c]	0.5	23.5	50.5	25.0	1.0	800
06DL71[c]	1.0	23.0	57.0	19.0	1.0	600
06DL73[c]	2.5	30.0	33.5	34.0	0.4	1700
06DL78[d]	n.d.	n.d.	5.0	95.0	160	700
06DL80[e]	n.d.	n.d.	5.0	95.0	60	1000

[a]Holocene lacustrine deposits (200 km SW of corridor B).
[b]Wadi el Qubba reddish silts bearing LDG.
[c]Corridor B reddish silts bearing LDG.
[d]Sand from the dune barcane between corridor A and B.
[e]Sand from the Great Sand Sea (80 km northward of the LDG site).

centimeter size. Coarse gravels were not analyzed. According to Clayton and Spencer (1934), the reddish silts are lacustrine in origin. Lacustrine deposits were thus analyzed from an ancient Holocene lake in the central Libyan Desert (06DL27: Fig. 1) for comparison with the silt-bearing LDG. As seen in Table 3, Holocene lacustrine deposits have a very high clay (kaolinite) content (75 wt%) with secondary quartz, whereas in the LDG area, the silts have a large quartz content (around 80 wt%) with secondary clay (dickite). In all these rock types, calcite, anhydrite, and/or gypsum are often below our detection limits.

The particle size distribution (Table 3) confirms the above-mentioned contrast between the Holocene lacustrine deposits and the LDG-bearing sediments. The high clay content of the Holocene lacustrine deposits accounts for the very fine particle size with 97.5 vol% <40 μm, whereas the Quaternary aeolian sands from the Great Sand Sea exhibit a very narrow range of grain size distribution (95 vol% >200 μm) without fine particles. The grain size distribution of the reddish silts from the Wadi el Qubba LDG site is rather comparable to that of the Holocene lacustrine deposits, but with a significant (20 vol%) sand contribution probably related to a fluvio-lacustrine mode of deposition, and a noticeable content of dickite, in place of kaolinite.

DISCUSSION AND CONCLUSIONS

LDG Fine Structure

Crystalline phases of SiO_2, like quartz or cristobalite, have unvarying IR parameters that allow one to determine their proportion in rocks (Pichard and Fröhlich 1986; Fröhlich 1989). Analysis of LDG samples and of other silica glasses of very different origin shows differences between their IR spectra that cannot be explained by the only slight variations found in their SiO_2 content. In particular, the IR wave number variations of the Si-O stretching band are known to be related to the mean Si-O-Si angle in silica glasses (Anand et al. 1995; Anand and Tomozawa 1997). In the same way, the wave number and the half-width of the Si-O-Si bending band, which are related, respectively, to the mean Si-O-Si angle value and to its scattering (Fröhlich 1989), account for differences in the (SiO_4) tetrahedral frameworks of the glasses. This is especially clear for the fulgurite and microelectronic fused quartz, which exhibit a large variation of the mean Si-O-Si angle and, in most cases, the highest values of the A and I spectral parameters (Table 1). In contrast, amorphous biogenic silica exhibits the lowest v, A, Δv, and I values. OH for O substitutions in this hydroxylated amorphous silica phase involve a deficit of Si-O and Si-O-Si vibrators; thus, A and I are lowered. According to Fröhlich (1989), $v_{[Si\text{-}O\text{-}Si]}$, which is a function of the mean Si-O-Si angle, is specific for the different silica phases (e.g., 800 cm^{-1} for amorphous biogenic silica, 798 cm^{-1} for quartz, 793 cm^{-1} for opal-CT, 790 cm^{-1} for tridymite; Fröhlich 1989). The mean Si-O-Si angle value is 143°7 for quartz (Le Page and Donnay 1976; Vieillard 1986) and 142°6 for amorphous biogenic silica, with a mean Si-O bond length of 1.62Å (Fröhlich 1989). Thus, taking into account the higher $v_{[Si\text{-}O\text{-}Si]}$ for LDG (804 cm^{-1} in average), it is inferred that its mean Si-O-Si angle is slightly <142°6 and the mean Si-O bond length > 1.62 Å.

The wave number of the mean Si-O-Si band angle for fused quartz is at 1101 cm^{-1} and for amorphous biogenic silica at 1100 cm^{-1}, but for LDG it shows higher values and varies markedly. This is related to differences in the mean Si-O-Si angle, and to differences in the mode of formation for these phases: at room temperature and by fixation of (SiO_4) tetrahedra on proteins for biogenic silica (Gendron-Badou et al. 2003), by a slow cooling of melted quartz for industrial silica, and perhaps by quenching melted quartz for

fulgurite and LDG. According to Krolikowski et al. (2009), due to the high pressure of the impact, the temperature of relaxation of LDG is lowered and the Si-O-Si angle is reduced. This is consistent with a higher value of the Si-O-Si band observed for all analyzed LDG. It is suggested here that the differences in the tetrahedral framework of these various glasses resulted from their different cooling histories and "fictive" temperatures (temperature of rigidification of the internal framework; Anand et al. 1995; Anand and Tomozawa 1997; Takada et al. 2009), related to cooling kinetics of glasses (Yue et al. 2002).

However, no clear correlations are seen in the wave number values between the bending Si-O-Si and stretching Si-O absorption bands, and only the **Ω** index shows significant differences between fulgurite and pure fused silica on the one hand (high values), and both the Great Sand Sea LDG and the Wadi el Qubba LDG on the other hand (low values). The Ω index is simply calculated as the ratio of intensities of the IR bands characteristic of intertetrahedral versus intratetrahedral links (Table 1). A high Ω value, such as for fulgurite and microelectronic glass (Table 2), is thus related to a small proportion of nonbridging oxygen atoms, and hence is an indication of a better polymerization of (SiO_4) tetrahedra than for Wadi el Qubba and Great Sand Sea LDG that exhibit lower Ω values. Ω is excessively low (3.84) for amorphous biogenic silica; this is related to the importance of defects in the three-dimensional tetrahedral framework, which is constituted of a discontinuous network of chains with an average of only six tetrahedra (Fröhlich 1989).

According to their Ω values, it is thus deduced that the LDG framework includes a rather high proportion of nonbridging oxygen atoms, and hence a high proportion of defects with regard to the continuous network of fused quartz. This may be related to the LDG's rather high Al, Ti, and Fe contents (0.2 to 1.2 wt% Al; 0.03 to 0.12% Ti; 0.03 to 0.18% Fe, according to Barrat et al. 1997), atoms that are occupying the defect sites (e.g., see the LDG cathodoluminescence study by Gucsik et al. 2004). The differences in the defect proportion might have induced differences in the Fe site coordination, which is known for LDG to be a mixture 4 and 5, 4.5 on average (Giuli et al. 2002, 2003). Small differences observed for specimens from the same area imply slightly variable PTt (pressure–temperature–time) conditions on a local scale. If the Great Sand Sea LDG and the Wadi el Qubba LDG originated from the same impact event, and also from the same target rocks, their Ω indices (respectively 4.23 and 4.14) probably indicate a slightly higher proportion of defects in the framework of the Wadi el Qubba LDG. The smaller size of the latter is compatible with a greater distance from the impact zone.

Finally, the frequent monazite relics in LDG, which were surely inherited from clastic sediments, confirm the terrestrial signature of the LDG REE content previously established by Rocchia et al. (1996, 1997).

Wadi el Qubba LDG Occurrence

Are the Wadi el Qubba LDG blocks in situ or were they transported here from the Great Sand Sea by Prehistoric men? Several observations and analyses are consistent with the assignment of this new LDG occurrence to the LDG strewn field.

1. The color (pink) of all the Wadi el Qubba specimens is quite different from the Great Sand Sea ones (yellow to green);
2. The size is considerably smaller (2–3 g against 60–2650 g);
3. The molecular structure is clearly slightly different (Table 1);
4. No large artifacts made from large LDG blocks, as in the Great Sand Sea, were found at Wadi el Qubba; mostly, local sandstones (a bad material for lithic industry) were used; only one small blade was found that was made from the same glass as the other LDG found in the neighborhood (size, color, molecular structure as indicated by their Ω index).

Thus, we infer that the Wadi el Qubba LDG blocks are in place and hence they are included in the LDG strewn field. The small size of the blocks is consistent with a distal position with regard to an impact zone in the Great Sand Sea area.

LDG Geological Environment

It is generally assumed that the silts bearing LDG are fluvial deposits (e.g., Clayton and Spencer 1939; Said 1990). The mineralogical and particle size distribution analyses displayed here give new information to refine their mode of deposition. The silt from corridor B exhibits a grain size distribution with a large grain size range, inconsistent with a wind or a lacustrine origin. The low clay fraction contribution (2.5 vol%) is, here, related to the coarse size of dickite crystals and probably also to a higher water energy in the depositional environment, as seen with the considerable sand fraction proportion. The silts carrying and coating the LDG blocks and infilling its tubes exhibit a mineralogical composition similar to that of the analyzed Mesozoic sandstones, but they are often enriched in dickite and may also have some minor kaolinite. The particle size distribution of these silt deposits (Table 3) and their mineralogical composition (Table 2) may well be derived from the mechanical

erosion of the dominantly Mesozoic dickite-bearing Gilf Khebir sandstone series, but including perhaps some of its kaolinite-bearing Paleozoic base. Holocene lacustrine deposits, which are essentially composed of kaolinite arising by the wind from southern lateritic soils overlying the metamorphic basement and exposed since Miocene times, are clearly different in origin.

The Wadi el Qubba silts exhibit a size distribution characteristic for both lacustrine and fluviatile modes, but with the same mineralogical composition as in the corridor B (quartz > 80 wt%; dickite < 20 wt%). Contrary to Holocene lacustrine deposits, kaolinite is absent at Wadi el Qubba. This is highly significant, as this clay appeared in sediments only from the early Miocene (Fröhlich 1981, 1982). At that time, a major global climatic change led to the transfer of kaolinite from the eroded lateritic soils to the sedimentary basins. This suggests a pre-Miocene age of the Wadi el Qubba silts.

Significant tectonic events occurred during the Oligocene epoch (Red Sea opening, formation of the East African Rift Valley, formation of the Dead Sea rift, etc.), including the Gilf Khebir uplift (Said 1983). During Oligocene and Miocene times, catastrophic floods (Brookes 2001) were responsible for severe erosion of the reliefs like the Gilf Khebir Plateau. During the Oligocene, one of the three main rivers that drained southwestern Egypt was the so-called Gilf River, which originated in the Gilf Khebir Plateau and ran northward (Goudie 2005). According to that paper, this drainage system included inland lakes and deltas. The fluvio-lacustrine deposits that had originated from the intense weathering and breakup of the Mesozoic "Nubian" sandstones were reworked by the wind during the Quaternary arid periods and gave rise to the Great Sand Sea sand sheet (El-Baz et al. 2000).

Thus, the geological setting of the LDG strewn field (including both Great Sand Sea and Wadi el Qubba sites) shows that LDG formation occurred just after the Gilf Khebir Plateau uplift and during its subsequent mechanical erosion by strong floods along the depression formed by the present Wadi al Malik and Wadi el Qubba valleys during the late Oligocene and Miocene times. The age of deposition of the reddish silts bearing LDG, which are cropping out within this large area and are covered northward by the Great Sand Sea sheet, is unknown, but we can infer from their mineralogical constitution and grain size distribution that they probably originate from the segregation and deposition of fine quartz grains (probably the microquartz cement of Mesozoïc sandstones) during this period. Then the environment of deposition of the reddish silts would be a fluvio-lacustrine complex: probably a large water sheet derived from the Gilf Khebir Plateau. Such a fluvio-lacustrine or lagoonal environment was previously determined for the LDG formation environment, on the basis of the high ^{7}Li isotope concentration in LDG (Magna et al. 2011).

LDG Rock Source

The silts bearing LDG exhibit a high clay mineral content (up to 25 wt%; Table 2) that cannot account for the near 100% silica content of LDG (96.5–99 wt%; 98.5 wt% on average; Spencer 1939; Diemer 1997; Fudali 1981; Koeberl 1997). Thus, the Libyan glasses did not originate from their soft sedimentary host material. Similarly, the Al-rich mineralogical composition of the Wadi el Qubba Turonian sandstones (about 10% dickite: Table 2) is incompatible with LDG chemical composition. The only rocks outcropping today that could have been the LDG source are the Turonian reddish sandstones and quartzites from the southern Great Sand Sea, which have nearly 100 wt% silica (Table 3). However, according to Schaaf and Müller-Sohnius (2002), the Cretaceous sandstones' Sr and Nd isotopic compositions are inconsistent with those of LDG. These authors infer that the target rocks could have been soft clastic rocks derived from the Precambrian crystalline basement.

Likewise, on the basis of $\delta^{18}O$ analysis, Longinelli et al. (2011) considered that the target rocks were quartz-rich sediments derived *directly* from weathered Pan-African intrusive rocks, the Cretaceous sandstones being different in $\delta^{18}O$. However, even though the Cretaceous sandstones are composed of quartz grains probably derived from weathered pan-African rocks, they are, as mentioned above, cemented with authigenic microquartz. Thus, their bulk $\delta^{18}O$ content would be significantly affected by that of the microquartz cement. The effect of erosion, including weathering, destruction, transport by rivers, and grain size segregation with regard to water energy during the deposition of the Cretaceous sandstones, would lead to the deposition of quartz sands.

It is thus deduced here that the LDG target was quartz sands that originated from the destroyed Cretaceous sandstones deprived of their microquartz cement, and deposited in a rather high-energy, fluviatile environment. The microquartz cement of the sandstones would have been deposited elsewhere (perhaps the reddish silts), in a lower energy, fluvio-lacustrine environment.

Acknowledgments—This research was undertaken in the framework of the ACI Programme "*Du chopper au brillant*," supported by the French Ministère de la Recherche et de l'Enseignement Supérieur. We thank Anne-Marie Brunet for the IR preparations, Michèle Destarac and Patrick Lafaite for their contribution to image presentation, Patrick Schmidt for his

improvements to the manuscript, P. Massare for useful remarks, Yannick Lefrais for his contribution to the SEM-EDX analyses, and Salah Abdessadok for grain size analyses. We thank also our desert guide, Mahmoud Nour el Din, and his team. We are grateful to Patrick Darphin for his expert organization of the expedition, and to all its members. Finally, we thank C. Koeberl, G. Giuli, P. Horn, and the anonymous MAPS reviewers for their excellent suggestions for the improvement of this paper.

Editorial Handling—Dr. Christian Koeberl

REFERENCES

Anand A. and Tomozawa M. 1997. Correlation of silica glass properties with the infrared spectra. *Journal of Non-Crystalline Solids* 209:166–174.

Anand A., Davis K. M., and Tomozawa M. 1995. A simple IR spectroscopic method for determining fictive temperature of silica glasses. *Journal of Non-Crystalline Solids* 185:191–198.

Barakat A. A., de Michele V., Negro G., Piacenza B., and Serra R. 1997. Some new data on the distribution of Libyan Desert Glass (Great Sand Sea, Egypt). In *Proceedings of the "Silica 96" Meeting on Silica Glass and related desert events, Bologna, July 1996*, edited by de Michele V. Milano: Pyramids. pp. 29–36.

Barnes V. E. and Underwood J. R. Jr. 1976. New investigations in the strewn-field of Libyan Glass and its petrography. *Earth & Planetary Science Letters* 30:117–122.

Barrat J. A., Jahn B. M., Amossé J., Rocchia R., Keller F., Poupeau G., and Diemer E. 1997. Geochemistry of Libyan Desert Glasses. *Geochimica & Cosmochimica Acta* 61:1953–1959.

Beran A. and Koeberl C. 1997. Water in tektites and impact glasses by fourier-transformed infrared spectrometry. *Meteoritics & Planetary Science* 32:211–216.

Bigazzi G., and de Michele V. 1997. New fission-track ages of Libyan Desert Glass. In *Proceedings of the "Silica 96" Meeting on Silica Glass and related desert events, Bologna, July 1996*, edited by de Michele V. Milano: Pyramids. pp. 49–57.

Bölitz M. C. and Langenhorst F. 2009. Liquid immiscibility and gas content in dark schlieren of Libyan Desert Glass (abstract #2018). 40th Lunar and Planetary Science Conference. CD-ROM.

Boslough M. B. E. and Crawford D. A. 2008. Low-altitude airbursts and the impact threat. *International Journal of Impact Engineering* 35:1441–1448.

Brookes I. A. 2001. Possible Miocene catastrophic flooding in Egypt's Western Desert. *Journal of African Earth Sciences* 32:325–333.

Clayton P. A. and Spencer L. J. 1934. Silica-Glass from the Libyan Desert. *Mineralogical Magazine* XXIII:501–508.

Diemer E. 1997. Libyan Desert Glass: An impactite. State of the art in July 1996. In *Proceedings of the "Silica 96" Meeting on Silica Glass and related desert events, Bologna, July 1996*, edited by de Michele V. Milano: Pyramids. pp. 95–109.

Duyckaerts G. The infrared analysis of solid substances. *Analyst* 84:201–214.

El-Baz F., Maingue M., and Robinson C. 2000. Fluvio-aeolian dynamics in the north-eastern Sahara: The relationship between fluvial/aeolian systems and ground-water concentration. *Journal of Arid Environments* 44:173–183.

Frischat G. H., Heide G., Müller B., and Weeks R. A. 2001. Mystery of the Libyan Desert Glasses. *Physics & Chemistry of Glasses* 42:179–83.

Fröhlich F. 1981. Les silicates dans l'environnement pélagique de l'océan Indien au Cénozoïque. Mémoire du Muséum National d'Histoire Naturelle Nouvelle série C Tome XLVI. 206 p.

Fröhlich F. 1982. Mineralogical evolution and stratigraphic correlations in azoic pelagic deposits from Indian ocean. *Bulletin de la Société Géologique de France* 7, XXIV:563–571.

Fröhlich F. 1989. Deep-sea biogenic silica: New structural and analytical data from infrared analysis—Geological implications. *Terra Nova* 1:267–273.

Fröhlich F. and Leclaire L. 1981. L'analyse minéralogique des sédiments associés aux nodules polymétalliques par la spectroscopie d'absorption infrarouge. Bulletin du Muséum National d'Histoire Naturelle, 4e sér., 3, C, n°2, Paris. pp. 159–181.

Fröhlich F., Poupeau G., Badou A., and Pleurdeau D. 2009. Une matière énigmatique: Le verre du désert Libyque. In *L'homme et le précieux–matières minérales précieuses*, edited by Moncel M.-H. and Fröhlich F. Oxford: British Archaeological Reports, International Series, 1934. pp. 55–66.

Fudali R. F. 1981. The major element chemistry of Libyan Desert Glass and the mineralogy of its precursor. *Meteoritics* 16:247–259.

Gendron-Badou A., Coradin T., Maquet J., Fröhlich F., and Livage J. 2003. Spectroscopic characterization of biogenic silica. *Journal of Non-Crystalline Solids* 316:331–337.

Gentner W., Storzer D., and Wagner G. A. 1969. Das Alter von Tektiten und verwandten Gläsern. *Naturwissenschaften* 56:255–260.

Giuli G., Pratesi G., Cipriani C., and Paris E. 2002. Iron local structure in tektites and impact glasses by extended X-ray absorption fine structure and high-resolution X-ray absorption near-edge structure spectroscopy. *Geochimica et Cosmochimica Acta* 66:4347–4353.

Giuli G., Paris E., Pratesi G., Koeberl C., and Cipriani C. 2003. Iron oxidation state in the Fe-rich layer and silica matrix of Libyan Desert Glass: A high-resolution XANES study. *Meteoritics & Planetary Science* 38:1181–1186.

Goudie A. S. 2005. The drainage of Africa since Cretaceous. *Geomorphology* 67:437–456.

Greshake A., Koeberl C., Fritz J., and Reimold W. U. 2010. Brownish inclusions and dark streaks in Libyan Desert Glass: Evidence for high-temperature melting of the target rock. *Meteoritics & Planetary Science* 45:973–989.

Gucsik A., Koeberl C., Branstätter F., Libowitsky E., and Zhang M. 2004. Infrared, Raman, and cathodoluminescence studies of impact glasses. *Meteoritics & Planetary Science* 39:1273–1285.

Horn P., Müller-Sohnius D., Schaaf P., Kleinmann B., and Storzer D. 1997. Potassium-argon and fission-tracks dating of Libyan Desert Glass, and strontium-neodynium isotope constraints on its source rock. In *Proceedings of the "Silica 96" Meeting on Silica Glass and related desert events, Bologna, July 1996*, edited by de Michele V. Milano: Pyramids. pp. 59–73.

Ip K. H., Stuart B. H., Ray A. H., and Thomas P. S. 2008. A spectroscopic investigation of the weathering of a heritage Sydney sandstone. *Spectrochemica Acta Part A* 71:1032–1035.

Kleinmann B. 1969. The breakdown of zircon observed in the Libyan Desert Glass as evidence of its impact origin. *Earth & Planetary Science. Letters* 5:497–501.

Kleinmann B., Horn P., and Langenhorst F. 2001. Evidence for shock metamorphism in sandstones from the Libyan Desert Glass strewn field. *Meteoritics & Planetary Science* 36:1277–1282.

Klitzsch E. 1990. Paleogeographical development and correlation of Continental Strata (former Nubian Sandstone) in northeast Africa. *Journal of African Earth Sciences (and the Middle East)* 10:199–213.

Klitzsch E., List F. K., and Pöhlmann G. 1987. *Geological map of Egypt 1:500 000, sheet NG 35 SW Wadi el-Qubba*. Cairo: The Egyptian Petroleum Corporation.

Koeberl C. 1997. Libyan Desert Glass: Geochemical composition and origin. In *Proceedings of the "Silica 96" Meeting on Silica Glass and related desert events, Bologna, July 1996*, edited by de Michele V. Milano: Pyramids. pp. 121–131.

Krolikowski S., Brungs S., and Wondraczek L. 2009. Relaxation of Libyan Desert Glass: Evidence for negative viscosity-pressure in silica? *Journal of Non-Crystalline Solids* 355:1666–1668.

Le Page Y., and Donnay G. 1976. Refinement of the crystal structure of low quartz. *Acta Crystallographica* 32:2456–2459.

Lecomte J. 1949. *Le rayonnement infrarouge*, vol. 2. Paris: Gauthiers-Villars ed. 754 p.

Longinelli A., Sighinolfi G., de Michele V., and Selmo E. 2011. $\delta^{18}O$ and chemical composition of Libyan Desert Glass, country rocks, and sands. New considerations on target material. *Meteoritics & Planetary Science* 46:218–227.

Magna T., Deutsch A., Mezger K., Skala R., Seitz H.-M., Mizera J., Randa Z., and Adolph L. 2011. Lithium in tektites and impact glasses: Implications for sources, histories and large impacts. *Geochimica and Cosmochimica Acta* 75:2137–2158.

Monod T., and Diemer E. 1997. A bibliography on Libyan Desert Glass. In *Proceedings of the "Silica 96" Meeting on Silica Glass and related desert events, Bologna, July 1996*, edited by de Michele V. Milano: Pyramids. pp. 19–26.

Parke S. 1974. Glasses. In *The infrared spectra of minerals*, vol. 4, edited by Farmer V. C. London: Mineralogical Society. pp. 483–514.

Pichard C. and Fröhlich F. 1986. Analyses infrarouges quantitatives des sédiments. Exemple du dosage du quartz et de la calcite. *Revue de l'Institut. Français du Pétrole* 41:809–819.

Pratesi G., Viti C., Cipriani C., and Mellini M. 2002. Silicate-silicate liquid immiscibility and graphite ribbons in Libyan Desert Glass. *Geochimica et Cosmochimica Acta* 66:903–911.

Rocchia R., Robin E., Fröhlich F., Meon H., Froget L., and Diemer E. 1996. L'origine des verres du désert libyque: Un impact de météorite. *Compte-Rendus de l'Académie des Sciences* 322:839–845.

Rocchia R., Robin E., Fröhlich F., Amossé J., Barrat J. A., Meon H., Froget L., and Diemer E. 1997. The impact origin of Libyan Desert Glass. In *Proceedings of the "Silica 96," Meeting on Silica Glass and related desert events, Bologna, July 1996*, edited by de Michele V. Milano: Pyramids. pp. 143–149.

Ruiz Cruz M. D. 1998. Kaolinite and dickite formation during shale diagenesis: Isotopic data. *Applied Geochemistry* 13:95–104.

Said R. 1983. Remarks on the origin of landscape of the eastern Sahara. *Journal of African Earth Sciences* 1:153–158.

Said R., ed. 1990. *The geology of Egypt*. Rotterdam, the Netherlands: A. A. Balkema. pp. 497–499.

Schaaf P. and Müller-Sohnius D. 2002. Strontium and neodymium isotopic study of Libyan Desert Glass: Inherited Pan-African age signatures and new evidence for target material. *Meteoritics & Planetary Science* 37:565–576.

Spencer L. J. 1939. Tektites and silica-glass. *Mineralogical Magazine* XXV 167: 425–440.

Storzer D. and Koeberl C. 1991. Uranium and zirconium enrichments in Libyan Desert Glass; zircon, baddeleyite, and high temperature history of the glass. Proceedings, 22nd Lunar and Planetary Science. pp. 1345–1346.

Storzer D. and Wagner G. A. 1977. Fission-track dating of meteorite impacts. *Meteoritics* 12:368–369.

Svetsov V. V. and Watson J. T. 2007. Melting of soil rich in quartz by radiation from aerial bursts—A possible cause of formation of Libyan Desert Glass and layered tektites (abstract #1499). 38th Lunar and Planetary Science Conference. CD-ROM.

Takada A., Richet P., and Atake T. 2009. New description of structural disorder in silica glass. *Journal of Non-Crystalline Solids* 355:694–699.

Vieillard P. 1986. Relations entre structure et parameters thermodynamiques des phases de silice. *Bulletin de Minéralogie* 109:219–238.

Weeks R. A., Underwood J. R. Jr., and Giegengack R. 1997. Libyan Desert Glass: A review. *Journal of Non-Crystalline Solids* 64:593–619.

Yue Y. Z., Christiansen J. de C., and Jensen S. L. 2002. Determination of the fictive temperature for a hyperquenched glass. *Chemical Physics Letters* 357:20–24.